ResearchGate

See discussions, stats, and author profiles for this publication at: https://www.researchgate.net/publication/280586728

A Polymer Brush Based Nanovalve Controlled by Nanoparticle Additives: Design Principles

ARTICLE *in* THE JOURNAL OF PHYSICAL CHEMISTRY B · JULY 2015

Impact Factor: 3.3 · DOI: 10.1021/acs.jpcb.5b02623 · Source: PubMed

READS

22

4 AUTHORS, INCLUDING:

Afshin Eskandari Nasrabad

University of Pittsburgh

17 PUBLICATIONS **238** CITATIONS

SEE PROFILE

Available from: Afshin Eskandari Nasrabad

Retrieved on: 27 January 2016

THE JOURNAL OF PHYSICAL CHEMISTRY B

Article

pubs.acs.org/JPCB

A Polymer-Brush-Based Nanovalve Controlled by Nanoparticle Additives: Design Principles

Rob D. Coalson,*[,†] Afshin Eskandari Nasrabad,[‡] David Jasnow,[‡] and Anton Zilman[§]

[†]Department of Chemistry and [‡]Department of Physics and Astronomy, University of Pittsburgh, Pittsburgh, Pennsylvania 15260, United States

[§]Department of Physics and Institute for Biomaterials and Biomedical Engineering, University of Toronto, Toronto, Ontario M5S 1A7, Canada

ABSTRACT: Polymer-grafted surfaces and channels are increasingly used for the design of responsive materials and sensors due to robust performance and ease of use. Various strategies for the control of the nanoscale morphologies of such materials and devices are being tested. Entropic repulsion between the polymer chains in a grafted brush of sufficient density causes the chains to extend in the direction perpendicular to the grafting surface in comparison to the position of unattached polymers. When nanoparticles having attractive interactions with the polymers are introduced into the solvent, these nanoparticles tend to infiltrate into the brush and reduce its extension. Under certain conditions, a sharp reduction in brush height extension can occur over a narrow range of nanoparticle concentrations in solution. We describe a way of controlling transport through polymer-functionalized nanochannels with nanoparticle additives, relying on the physics of nanoparticles and polymer brushes under confinement, and we suggest a blueprint for the creation of a tunable nanovalve. The nanovalve is modeled as a cylinder with a polymer brush grafted on its inside surface. Brush properties such as the chain length and the grafting density are chosen so that the brush chains extend into the center of the cylinder in the absence of nanoparticles, occluding the flux of analyte molecules through the pore. When nanoparticles that are attracted to the polymers are introduced into solution, they infiltrate into the brush and partially collapse it against the cylindrical grafting surface, opening space in the center of the cylinder through which analyte molecules can flow. The operation of such a nanovalve is analyzed via self-consistent field theory calculations in the strong-stretching approximation. Self-consistent field analysis is supported by Langevin dynamics simulations of the underlying coarse-grained model of the polymer−nanoparticle system.

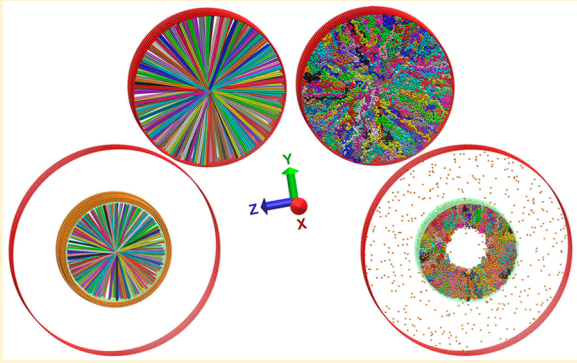

Downloaded by UNIV OF PITTSBURGH on September 3, 2015 | http://pubs.acs.org
Publication Date (Web): August 21, 2015 | doi: 10.1021/acs.jpcb.5b02623

1. INTRODUCTION

A polymer brush is an array of polymer chains tethered at one end to a grafting surface.[1,2] Polymer brushes have many interesting morphological properties, making their behavior rather distinct from that of untethered polymers in solutions and melts.[3−6] For example, the extent ("height") of a typical brush layer scales proportionally to the number of monomers in a chain, N, in contradistinction to the end-to-end distance of an untethered polymer, which is proportional roughly to $N^{3/5}$.[7] This extended conformation of the polymer brush leads to an inherent tendency to resist compression. This property can be exploited by coating solid surfaces (e.g., of pipes) with grafted polymers to prevent other molecules in the solution from adhering to and thus "fouling" the surface and for a variety of nanofluidics applications.[8−10] Additionally, the unique mechanical properties of the brush under compression make polymer-brush coatings of interest for tribology and lubrication.[4,11]

Molecular additives, i.e., molecules or nanoinclusions from solution that partition into the brush, can affect the properties of the brush (e.g., its stiffness) in such a way as to modify its tribological and antifouling properties.[3,6,12] For instance, if the molecular additives induce a strong degree of swelling or compression in the brush height,[13] this effect could be exploited for nanosieving applications.[14−16] As a concrete example, consider an impenetrable wall into which a small cylindrical pore (e.g., less than 1 μm in diameter) has been drilled. One could coat the inside of the pore with a polymer brush material and make the polymer strands long enough that, in the absence of chemical additives, the brush extends to the center of the pore and hence impedes the passage of molecules dissolved in solution. Such polymer-coated channels have been realized for applications in molecular sorting, DNA detection, and more.[17−22] The addition of nanoparticles with appropriately chosen properties will lead to their infiltration into the brush and may cause it to contract toward the walls under appropriate conditions. If the contraction is sufficient, enough unoccluded space will open along the cylinder axis to let analytes up to a certain size pass through. Sharp transitions in the brush height

Received: March 18, 2015
Revised: July 6, 2015
Published: July 29, 2015

ACS Publications © 2015 American Chemical Society

DOI: 10.1021/acs.jpcb.5b02623
J. Phys. Chem. B 2015, 119, 11858−11866

Downloaded by UNIV OF PITTSBURGH on September 3, 2015 | http://pubs.acs.org
Publication Date (Web): August 21, 2015 | doi: 10.1021/acs.jpcb.5b02623

induced by the nanoparticles allow precise control of the channel selectivity.

In recent work, we have developed a statistical mechanical model with an analytical component supported by coarse-grained simulations that provides guidance into the phenomenon of sharp polymer-brush collapse induced by attractive nanoparticle inclusions.[23,24] An important theoretical tool for our statistical mechanical model has been the version of self-consistent field theory (SCFT) introduced by Semenov;[25] Zhulina and co-workers;[26] and Milner, Witten, and Cates[27] known as strong-stretching theory (SST).[7,28−32] In the present paper, we extend our work on planar brushes with attractive nanoparticle inclusions to the case of an inside-grafted cylindrical brush to investigate the feasibility of creating a tunable nanovalve based on these principles.

2. METHODS: STRONG-STRETCHING THEORY FOR AN INSIDE-GRAFTED CYLINDRICAL BRUSH IN THE PRESENCE OF ATTRACTIVE NANOPARTICLE INCLUSIONS

SST has been mostly used for plane-grafted polymer brushes,[2,26,27,33,34] although extensions to curved surfaces have been studied.[35−37] In recent work, we generalized this theory to treat the case in which attractive nanoparticles were added to the system.[23,24] The nanoparticles partition between a bulk solution phase, which is characterized by a specified nanoparticle concentration, and the tethered polymer brush. Energetic and entropic effects associated with nanoparticle infiltration into the brush can give rise to pronounced morphological changes that do not occur in the absence of the nanoparticles. In subsection 2.1 below, we outline general aspects of the SST approximation for an inside-grafted cylindrical brush based on the development given by Manghi et al.[37] for a system with no nanoparticles. In subsection 2.2, we give a specific form of the free-energy density that includes the nanoparticles in the theory.

2.1. Strong-Stretching Theory for an Inside-Grafted Cylindrical Brush: General Structure. Consider a cylindrical channel containing an inside-grafted polymer brush with uniform surface-grafting density (average number of chains per unit area), as schematically depicted in Figure 1. At

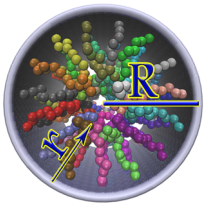

Figure 1. Schematic view of the cylindrical nanovalve of radius R with polymer chains grafted to the inside wall. By convention, we measure r from the value of 0 at the grafting surface to R at the cylinder center.

equilibrium, the average brush profile (as quantified by the monomer density) exhibits cylindrical symmetry. Presuming the channel to be long enough that the edge effects associated with the cap regions of a finite cylinder[38] are negligible, the average volume fraction of the monomers, ψ, is a function of the radial distance r only, i.e., $\psi = \psi(r)$. Note that we will measure r as the distance from the cylinder wall ($r = 0$ corresponds to the location at the wall); cf. Figure 1. The self-consistent field experienced by a monomer within SST,[26,27] denoted here as $\mu = \mu(\psi(r))$, is a function of the local monomer density. An explicit form of the function $\mu(\psi)$, including effects due to the presence of nanoparticles in solution, is provided in subsection 2.2. In SST, the mean field trajectory in space of each individual polymer, $r(s)$, is described by an equation analogous to the motion of a classical particle in an effective potential $V_{cl}(r) = -\mu(\psi(r))$; namely: $\ddot{r}(s) = -dV_{cl}(r(s))/dr$, where a key property of the motion is that a particle released from rest (corresponding to the ungrafted polymer end) at any value of r must reach the surface $r = 0$ at the time $s = N$. This "equal time" condition is only fulfilled by the harmonic potential $V_{cl}(r) = Br^2 - A$ with $B = \pi^2/(8N^2)$. The constant A becomes a normalization condition determined by the total number of monomers in the system and the polymer grafting density.[27] For convenience, we set the monomer size to 1. Thus, all lengths referred to in the SST formulas and calculations presented herein are in units of the monomer size.

Given a value of A, the monomer density profile $\psi(r)$ is uniquely determined by the relation

$$\mu(\psi(r)) = A - Br^2 \tag{1}$$

For polymer chain length N and surface grafting density σ, A is determined from the condition

$$\int_0^h (R - r)\psi(r)dr = N\sigma R \tag{2}$$

Here, h is the brush height (the value of r at which the brush terminates), which is related to A through eq 1. In practice, the solution is found by adjusting the value of A to satisfy eq 2 for specified values of N, σ, and R. This gives rise to a unique solution for the brush density $\psi(r)$.

Interpretation of the SST results in cylindrical geometry requires care because the values $h > R$ cannot be accommodated in eq 2 and within SST in general. In SST, the monomer density is maximal at the grafting surface and decreases monotonically with the distance from it. The extension of a brush that is not under compression is determined by the balance of pressure at the brush-solution interface. For a particular shape of $\mu(\psi)$, the osmotic pressure of the brush becomes equal to the osmotic pressure of the bulk solution[23,24] at a certain value of ψ, denoted as ψ^*. It will thus extend until the value of the monomer density becomes ψ^*, at which point the brush terminates at a distance $h^* = ([A - \mu(\psi^*)]/B)^{1/2}$ from the surface if $h^* < R$; in this case, the brush filaments extend from the grafting surface but do not reach the center of the cylinder. However, for sufficiently large A values, one finds $h^* > R$. This would mean that brush filaments extend beyond the point $r = R$, implying interdigitation, which cannot be accommodated in SST theory. Within the framework of this theory, filaments extending in from opposite sides of the pore act as an effective wall, preventing the penetration of any brush filament beyond.[37] This situation is analogous to bringing two plane-grafted brushes into contact at their nongrafted edges. In both cases, these edges come under compression and terminate sharply at the point of contact at a nonzero value of ψ.[27] Our simulations show that in the regime of interest, the actual degree of interdigitation is small (cf. Figure 5b below), supporting the validity of the SST approximation.

To summarize the computational procedure, we define the function $I(A) \equiv \int_0^h (R - r)\psi(r)dr$, where $h = \min\{R, ([A - \mu(\psi^*)]/B)^{1/2}\}$ is the brush height. The function $I(A)$ increases

DOI: 10.1021/acs.jpcb.5b02623
J. Phys. Chem. B 2015, 119, 11858−11866

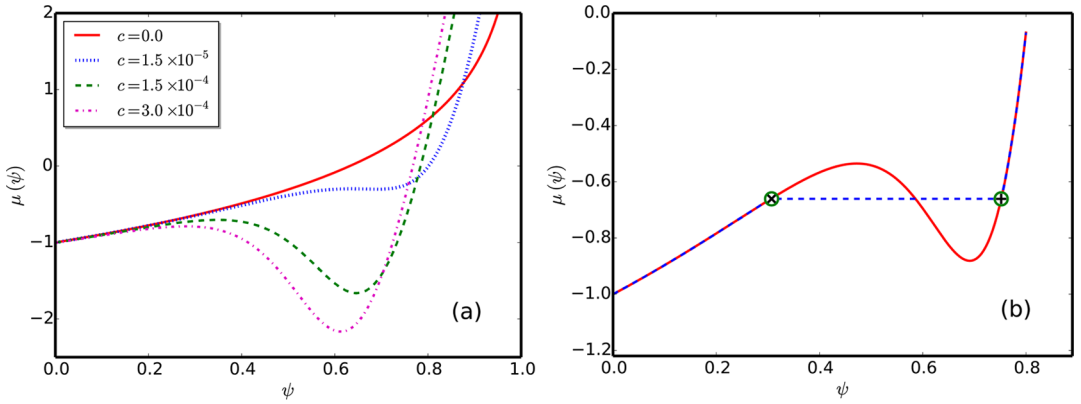

Figure 2. Self-consistent field $\mu(\psi)$ vs monomer density ψ. Left panel: the mean field $\mu(\psi)$ of eq 6 is plotted for four values of c at $\chi = -13.5$. The concentration regime in which there is an excisable van der Waals (vdW) loop extends from $c_1^* \approx 1.5 \times 10^{-5}$ to $c_2^* \approx 1.5 \times 10^{-4}$. Right panel: illustrative example of nanoparticle concentration $c = 5 \times 10^{-5}$ that falls within the excisable van der Waals loop regime. The self-consistent field $\mu(\psi)$ vs ψ is shown via solid red line. The application of a Maxwell equal-areas construction to excise the vdW loop generates the corrected $\mu(\psi)$ curve shown via the dashed blue line. In this illustrative example, $\psi_l = 0.31$ (cross with green circle) and $\psi_h = 0.75$ (plus sign with green circle).

Downloaded by UNIV OF PITTSBURGH on September 3, 2015 | http://pubs.acs.org
Publication Date (Web): August 21, 2015 | doi: 10.1021/acs.jpcb.5b02623

monotonically with A, resulting in a unique value of A that satisfies the normalization constraint $I(A) = N\sigma R$.

2.2. Details of the Non-Elastic Free Energy Density and SCF Potential. The local non-elastic free energy density can be expressed directly in terms of the local volume fractions of the monomers and the nanoparticles (denoted as $\psi(\vec{r})$ and $\phi(\vec{r})$, respectively) and can be inferred from a uniform macroscopic phase characterized by the chosen values of ψ and ϕ. Here, we present details for the case in which the volume of a nanoparticle is equal to that of a monomer, i.e., for $\bar{v} = 1$, where $\bar{v} \equiv$ (nanoparticle volume)/(monomer volume). Corresponding formulas for the more general case of $\bar{v} \neq 1$ can be found in ref 24.

The non-elastic free energy density of the brush−nanoparticle mixture, calculated in the lattice gas approximation is given in units of kT by[23,24]

$$f(\psi, \phi) = \phi \ln \phi + (1 - \psi - \phi) \ln(1 - \psi - \phi) + \chi\psi\phi \tag{3}$$

The first two terms in eq 3 reflect the translational entropy of the nanoparticles and the solvent molecules, respectively, with excluded volume constraints. In a standard derivation based on the Flory−Huggins theory, a term $\psi \ln \psi$ has been subtracted from the standard two-component lattice gas free-energy density, as this term represents the translational entropy of the monomers, which in fact are linked together into grafted polymer strands.[39,40] This term is then replaced by a term associated with the elastic-stretching free energy of the polymers, which ultimately leads to the "equations of motion" of Section 2.1. The final term on the right-hand side of eq 3 accounts for short-range monomer−nanoparticle interactions, treated within the random mixing approximation. The coupling strength χ is negative when the monomers are attracted to nanoparticles and is related to the second virial coefficient of the monomer−nanoparticle interaction.[7,23,24] The free-energy density proposed in eq 3 constitutes a minimal model. For example, binary interactions (other than hard-core excluded-volume interactions) of the monomer−monomer and nanoparticle−nanoparticle types are neglected here for simplicity. Additionally, all cubic and higher order attractive couplings between monomers and nanoparticles are ignored, as are electrostatic interactions, which are often present in systems of this type. Nevertheless, the model in eq 3 provides a good starting point for investigation of the morphological properties of a nanoparticle-infiltrated polymer brush, as verified by statistical mechanical simulations.[23,24]

Given eq 3, the nanoparticle chemical potential is given by

$$\mu_{np} = \partial f(\psi, \phi)/\partial\phi = \ln \phi - \ln(1 - \psi - \phi) + \chi\psi \tag{4}$$

At equilibrium, the chemical potential of the nanoparticles must be the same everywhere in the system. This means that at equilibrium, the local value of the nanoparticle concentration $\phi(r)$ depends on the local value of the monomer density $\psi(r)$ in accord with eq 4. The value of μ_{np} must be equal to the chemical potential of the nanoparticles in solution, which can be determined from eq 4 by setting $\psi = 0$ and the nanoparticle volume fraction equal to its bulk solution value, denoted as c. Specifically, the nanoparticle chemical potential is $\mu_{np} = \ln[\gamma(c)]$, $\gamma(c) \equiv c/(1 - c)$. In general, this is the chemical potential of a nonideal solution within a lattice gas approximation. However, in most experimentally relevant cases $c \ll 1$, in which case $\mu_{np} \cong \ln(c)$, i.e., the solution is essentially ideal. Denoting the local equilibrium nanoparticle density as $\bar{\phi}(\psi)$, eq 4 solves to

$$\bar{\phi}(\psi) = \frac{\gamma(1 - \psi)}{\gamma + \exp\{\chi\psi\}} \tag{5}$$

Clearly, $\bar{\phi}(\psi)$ is parametrically dependent on the solution-phase nanoparticle volume fraction c, as are the formulas for $\mu(\psi)$ and the osmotic pressure $P(\psi)$ presented below. Now we can deduce the SCF potential experienced by the monomers, $\mu(\psi)$, for this model, according to the relation[24]

$$\mu(\psi) = \left.\frac{\partial f(\psi,\phi)}{\partial\psi}\right|_{\phi=\bar{\phi}(\psi)} = -\ln(1 - \psi - \bar{\phi}(\psi)) + \chi\bar{\phi}(\psi) - 1 \tag{6}$$

To further understand the details of the SST procedure, it is useful to examine the shape of the $\mu(\psi)$ curve for several values of the nanoparticle solution volume fraction c, taking $\tilde{v} = 1$ so that eqs 5 and 6 apply directly. (Note: For $\bar{v} = 1$, the nanoparticle volume fraction and the nanoparticle concentration in units of (monomer size)$^{-3}$ are the same.) This is done in Figure 2. For small nanoparticle concentrations, the $\mu(\psi)$ curve increases monotonically with ψ in the region $0 < \psi$

DOI: 10.1021/acs.jpcb.5b02623
J. Phys. Chem. B 2015, 119, 11858−11866

< 1. To implement the SST procedure in this case, one simply picks a value of $A > \mu(0)$, appeals to eq 1 to determine $\psi(r)$, checks the normalization condition in eq 2, and adjusts A until this condition is satisfied. However, at some critical value of c (termed here c_1*) a van der Waals loop appears in the $\mu(\psi)$ versus ψ curve. This loop must be excised by a Maxwell equal-areas construction to remove unphysical regions within the loop region where the curve is nonmonotonic,[41] resulting in a horizontal tie-line in the corrected $\mu(\psi)$ curve that extends from a low-value ψ_l to a high-value ψ_h (cf. Figure 2). These two values of monomer density correspond to the same osmotic pressure, defined by

$$P(\psi) = \psi \left.\frac{\partial f(\psi,\phi)}{\partial \psi}\right|_{\phi=\bar{\phi}(\psi)} + \bar{\phi}(\psi) \left.\frac{\partial f(\psi,\phi)}{\partial \phi}\right|_{\phi=\bar{\phi}(\psi)} - f(\psi,\bar{\phi}(\psi)) = -\psi + \chi\psi\bar{\phi}(\psi) - \ln(1-\psi-\bar{\phi}(\psi)) \quad (7)$$

where the second equality in eq 7 holds for the specific non-elastic free-energy density function adopted in eq 3.

As c increases further, the value of ψ_l decreases until we reach a point where $\psi_l = 0$. Denote the volume fraction at which this happens as c_2*. For nanoparticle volume fractions $c > c_2$*, the Maxwell construction cannot be carried out in the region $0 < \psi < 1$. In this region, $\mu(\psi)$ versus ψ must be restricted to values of ψ greater than ψ*, such that $P(\psi^*) = P(0)$. In the region $\psi > \psi^*$, $\mu(\psi)$increases monotonically with ψ, and the SST procedure can be carried out in the usual manner.[26,27]

2.3. Coarse-Grained Simulations of a Polymer Brush Grafted to the Inside of a Cylinder in the Presence of Attractive Nanoparticles. To augment and verify the analytical theory, we have constructed a coarse-grained model of the brush−nanoparticle system and performed Langevin dynamics simulations on this system. The simulation procedure is analogous to the one we used previously to study a plane-grafted polymer brush.[23,24] Briefly, the polymer is represented by a chain of spherical monomers connected by finitely extensible nonlinear elastic (FENE) springs.[42] One end of the polymer is grafted to an inert support surface (here, the inside wall of a cylinder of radius R). The polymer brush consists of a randomly spaced array of grafted polymer chains, each N monomers in length, with an average surface density of grafting points set to the desired value σ. Excluded-volume interactions between all monomers are also encoded via appropriate Lennard−Jones-type pair potentials, as are the attractive interactions between polymer monomers and spherical nanoparticles that are introduced into the simulation box. The details of the microscopic potentials have been described in refs 23 and 24. Once the initial configuration is constructed, Langevin dynamics simulation is then carried out; we have tested a large number of initial conditions to make sure that we obtain the accurate equilibrium averages in the simulations. In the process, the attractive nanoparticles partition into the brush and under appropriate conditions partially collapse it, as illustrated in the Results section below.

3. RESULTS: A BRUSH-BASED NANOVALVE CONTROLLED BY NANOPARTICLE ADDITIVES

Consider an inside-grafted cylindrical brush with a specified chain length (N monomers per chain), grafting density σ, and radius R such that the brush filaments reach all the way from the grafting surface to the center of the cylinder in the absence of attractive nanoparticles. Now consider the addition of attractive nanoparticles (i.e., nanoparticles that are attractive to monomers of the polymer chains). As the concentration of nanoparticles in solution is increased, the brush will begin to retract, thus reducing the equilibrium value of the brush height. At some concentration value, the brush filaments will no longer reach all the way into the center of the pore. As this process continues, more free volume opens in the center of the cylinder. By exploiting the significant and sharp collapse of the brush that can be achieved in the model with appropriate choices of system parameters, one can precisely control the degree of retraction of the polymer strands. We put these ideas through rigorous testing using the combination of the analytical theory and the simulations described above.

As a starting point, we turn to previously studied behavior of the planar brush to guide the initial choice of the parameters for the cylindrical geometry. In particular, we choose $N = 100$, $\bar{v} = 1$, a grafting distance between chains $a = 4$ (so that $\sigma = 1/4^2 = 0.0625$), and $\chi = -13.5$. All lengths are measured in units of the monomer diameter. As shown in Figure 1 of ref 24, a plane-grafted brush characterized by these parameters undergoes strong collapse when nanoparticles are introduced into solution: a reduction of the brush height by a factor of approximately 5 occurs abruptly at nanoparticle volume fraction $c \approx 10^{-4}$. The pure brush (no nanoparticles) has a brush height $h_0 \approx 43.5$ in the plane-grafted geometry. For the cylindrical analog, we seek a system where the polymer strands extend into the center of the cylinder (to form a "closed valve" that has no free volume in its center) but do not extend significantly beyond the center (to minimize the possibility that interdigitating brush filaments will not retract toward the cylinder walls when attractive nanoparticles are added). We expect this situation to occur when $h_0 \approx R$. Hence, we set $R = 45$ for our cylinder. Results for the brush monomer density $\psi(r)$ when $c = 0$ are shown in Figure 3a, along with the $\psi(z)$ profile in the corresponding plane-grafted system. Note that $\psi(r)$ for the cylindrical brush terminates abruptly at $r = R$, with $\psi(r = R) > 0$. Clearly, there is no free volume (defined here as a region where $\psi = 0$) inside the cylinder in this system.

As the concentration of nanoparticles in solution c is increased, the brush starts to contract. In Figure 3b, we show results for $c = 1 \times 10^{-4}$. (The degree of nanoparticle infiltration into the brush depends on the nanoparticle chemical potential in the solution phase that is in contact with the cylindrical pore. This chemical potential is a monotonically increasing function of the nanoparticle concentration in the bulk solution.) Again, we show both $\psi(r)$ for the cylinder and $\psi(z)$ for the corresponding plane-grafted brush. The brush now extends only to $r \approx 33$, leaving some free volume in the center between $r = 33$−45. Upon increasing the nanoparticle concentration slightly further to $c = 1.5 \times 10^{-4}$, brush retraction becomes more pronounced, as shown in Figure 3c. Now the brush only extends to $r \approx 10$, opening significant free volume (from $r = 10$−45) in the center of the cylinder. For completeness, we have collected in Figure 3d the monomer profiles $\psi(r)$ for the cylindrical brush computed for the three cases discussed above. We note that the overall collapse effect here is similar to that predicted in previous computational studies[43] in a mixture of a bad solvent (which favors collapsed brush filaments) and a good solvent (which favors extended brush filaments). However, the physical mechanism of the collapse is quite

Downloaded by UNIV OF PITTSBURGH on September 3, 2015 | http://pubs.acs.org
Publication Date (Web): August 21, 2015 | doi: 10.1021/acs.jpcb.5b02623

DOI: 10.1021/acs.jpcb.5b02623
J. Phys. Chem. B 2015, 119, 11858−11866

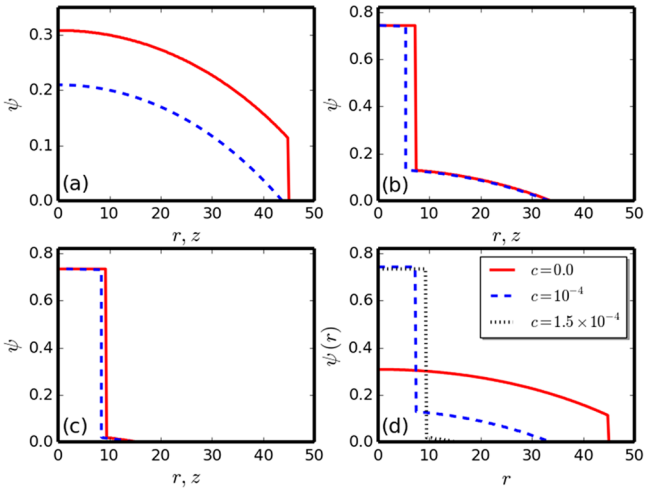

Figure 3. Monomer density profile ψ for different nanoparticle concentrations computed from SST: (a) $c = 0$, (b), $c = 10^{-4}$, and (c) $c = 1.5 \times 10^{-4}$. System parameters are $N = 100$, $\chi = -13.5$, $\sigma = 0.0625$, and $\overline{v} = 1$, and for the cylindrical brush the radius is $R = 45$. In these panels, the blue dashed curve shows the result for the plane-grafted system, and the solid red line shows the result for the corresponding inside-grafted cylindrical brush. Panel d compares the results for the monomer density profile of the cylindrical brush obtained at the three solution-phase nanoparticle concentrations considered in panels a–c.

different: in the case of a bad solvent, the collapse is triggered by expulsion of the bad solvent from the polymer-occupied region, whereas in the case of attractive nanoparticles, these particles partition into the brush region and trigger the retraction of the brush filaments around them. The possibility raised here of using attractive nanoparticles as the agents of collapse expands the array of options available for experimentally observing the effect and exploiting it for technological applications.

We plot in Figure 4 the brush height versus the solution-phase nanoparticle volume fraction calculated from the SST approximation for both cylindrical and planar geometries. For a "pure brush" (no nanoparticles), as discussed above, the plane-grafted brush has a height $h \approx 43.5$. Due to the curvature of the cylinder, the analogous cylindrically grafted brush extends out a

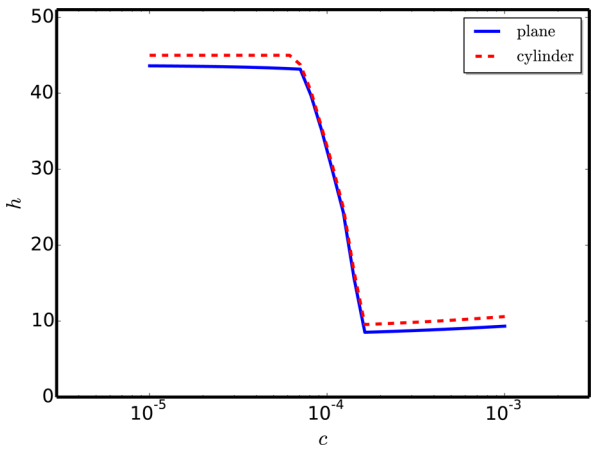

Figure 4. Brush height h vs nanoparticle volume fraction for the plane-grafted brush and the inside cylinder-grafted brush, calculated via SST. System parameters are $N = 100$, $\chi = -13.5$, $\sigma = 0.0625$, and $\overline{v} = 1$, and for the cylindrical brush the radius is $R = 45$.

little further: it reaches $h = R = 45$ and stops there (no brush end interdigitation occurs in the SST approximation). Both brushes contract sharply over the same narrow range of nanoparticle concentrations.

The range of nanoparticle concentrations over which the rapid decrease in brush height occurs falls in the regime where there is an excisable van der Waals loop in the mean field theory (MFT) monomer self-consistent field $\mu(\psi)$. In this regime, for nanoparticle concentrations close to c_2*, the brush morphology consists of a compact high-monomer-density component next to the grafting surface with a low-density tail extending out to free end of the brush. As c increases, the tail portion diminishes at the expense of the expanding high-density portion of the brush; see the monomer density plots in Figure 3. Eventually (for nanoparticle concentrations above c_2*), the brush becomes dense with no diffuse tail; with further increase of the solution nanoparticle concentration, c, the brush begins to swell. As expected intuitively, once the brush has retracted significantly away from the cylinder center, differences between the plane-grafted and cylinder-grafted systems are modest.

To verify the basic mechanism proposed on the basis of SST calculations, we have also performed coarse-grained polymer simulations as described in section 2.3 above. In these simulations, each polymer chain is 100 monomers in length and is grafted at one end to the inside surface of a cylinder corresponding to $R = 45$ (lengths are measured in units of the monomer diameter). As described above, chains are randomly grafted to the inside of the cylinder, such that the average surface density of grafted points is $\sigma = 1/4^2 = 0.0625$. The cylinder length is 23.2. Nanoparticles are initially placed outside of the cylindrical brush system as described below. Then molecular dynamics (MD) simulations with a Langevin thermostat[44] are performed using the LAMMPS software package[45] with underdamped Langevin dynamics.

Because our analytical model consists of a cylindrical pore system that is infinite in extent along the cylinder axis, we employed the simulation configuration illustrated in Figure 5c,d to enable nanoparticle infiltration into the brush from an external reservoir characterized by a bulk solution-phase nanoparticle concentration. Namely, we constructed a second, concentric confining cylinder with radius larger than that of the cylindrical pore (i.e., larger than R). Nanoparticles were placed in the annular region between the two cylinders. These nanoparticles were allowed to partition through the walls of the nanopore cylinder into the region where the polymer chains are grafted. Monomers of the polymer were *not* allowed to permeate into the nanoparticle reservoir region beyond the nanopore wall. Using this configuration, periodic boundary conditions in the cylinder axis direction can be applied, thus removing edge effects at the caps of the cylinder and reducing the size of the simulation system needed to effectively attain the infinite cylinder limit. Once nanoparticle partitioning is complete, i.e., equilibrium has been attained, we can count the average number of nanoparticles in the reservoir region to deduce the relevant bulk nanoparticle concentration.

As is clearly seen from Figure 5, when a sufficient number of nanoparticles partitions into the brush, the brush does indeed contract, thus confirming the mechanism predicted by our SST calculations above. To further quantify our simulation results, we show in Figure 6 h versus c profiles extracted from simulations for $\overline{v} = 1$ nanoparticles in the plane-grafted and cylinder-grafted systems described above with $\varepsilon_b = 2$, $N = 100$, and $R = 45$ for the cylindrical brush system, i.e., the system

Downloaded by UNIV OF PITTSBURGH on September 3, 2015 | http://pubs.acs.org
Publication Date (Web): August 21, 2015 | doi: 10.1021/acs.jpcb.5b02623

DOI: 10.1021/acs.jpcb.5b02623
J. Phys. Chem. B 2015, 119, 11858–11866

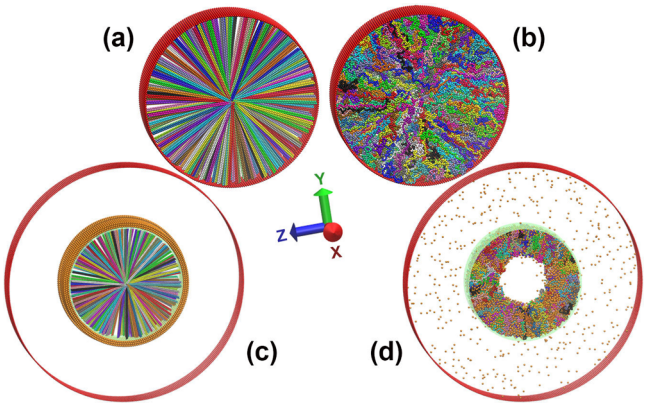

Figure 5. Simulation snapshots of inside-grafted cylindrical brushes for a cylinder with radius R = 45 shown from an end-on view. (The actual length of the simulation cylinder is 23.2 in units of the monomer diameter.) Panels a and b pertain to the case that c = 0 (no nanoparticles). Panel a shows a typical initial configuration prior to Langevin dynamics simulation. Panel b shows a snapshot of the system after equilibrium has been attained. Note that the polymer chains fill the entire volume within the cylinder ($\psi > 0$ everywhere) and that the degree of extension of a given polymer chain beyond the cylinder center is small. Panels c and d pertain to the case in which the nanoparticle volume fraction is c = 0.007 after equilibration. In our simulation procedure, the solution-phase nanoparticles are confined to a second cylindrical region exterior to the grafting cylinder radius R and are allowed to permeate into the brush through the grafting wall. Panel c shows the initial configuration of polymers chains and nanoparticles (small brown spheres packed around the outside of the grafting surface). Panel d shows a snapshot of the system after equilibrium has been attained. Infiltration of the attractive nanoparticles into the brush causes it to retract toward the grafting surface, leaving significant open space (ψ = 0) in the center of the cylinder.

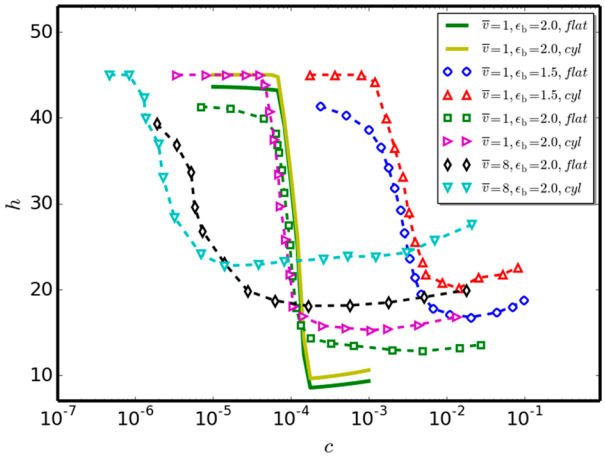

Figure 6. Effect of the binding strength and particle size on the brush collapse for the plane-grafted brush and the inside-grafted cylinder brush. Open symbols connected by dashed lines signify values obtained from Langevin dynamics simulations; solid lines indicate SST results. In all cases, the chain length is N = 100, and the relevant cylinder radius is R = 45. Simulation results for plane-grafted vs inside-grafted cylinder brush are presented for several choices of $\overline{v}$ and ε_b, as detailed in the figure legend. As established in ref 24, for a $\overline{v}$ = 1 nanoparticle, the nanoparticle−monomer binding strength ε_b = 2.0 corresponds to a mean-field coupling strength of χ = −13.5. Thus, the case $\overline{v}$ = 1, ε_b = 2.0 corresponds directly to the system analyzed by SST in Figures 2−4.

parameters used in Figure 3 above. Note that in the simulations we compute the solution-phase nanoparticle volume fraction c as $c = \rho\overline{v}$, where ρ = nanoparticle number density in units of b^{-3}, with b being the Lennard−Jones diameter of a polymer monomer. To further characterize the collapse process illustrated in Figure 5, we also show in Figure 6 the corresponding results for two additional systems. Specifically, we consider a system with a lower value of the nanoparticle-monomer binding strength ε_b = 1.5 (and $\overline{v}$ = 1, σ = 0.0625, and N = 100) and a second system with larger nanoparticles, characterized by $\overline{v}$ = 8 (and ε_b = 2, σ = 0.0625, and N = 100).

Focusing first on the case of $\overline{v}$ = 1 (and ε_b = 2, σ = 0.0625, and N = 100), we note that it was established in ref 24 that the nanoparticle−monomer binding strength ε_b = 2 in the simulations corresponds to the MFT nanoparticle−monomer coupling strength χ = −13.5. The SST predictions (cf. Figure 4) for this system are replotted alongside the corresponding Langevin simulation results in Figure 6; semiquantitative agreement with the corresponding SST predictions is apparent. The SST approximation generally predicts sharp features that the full simulation smooths out. In the case of the h versus c curves, the decrease observed in the simulations is not quite as sharp (occurs over a slightly wider range of nanoparticle concentrations), and the collapse is not quite as deep.

Next we consider the system with weaker nanoparticle−-monomer binding strength ε_b = 1.5 (all other parameters being the same as the case described in the previous paragraph). The h versus c curves shown for both plane-grafted and cylinder-grafted brushes in Figure 6 indicate less brush contraction than is achieved when ε_b = 2 and require higher nanoparticle concentrations to generate the contraction. This is expected given the smaller degree of nanoparticle−monomer attraction. These results illustrate how the nanoparticle binding strength can be tuned to produce nanovalves with varying degrees of maximum compression and different nanoparticle concentration regimes of operation.

Returning now to the system with ε_b = 2, σ = 0.0625, and N = 100, but featuring a larger nanoparticle, namely one having volume $\overline{v}$ = 8, one sees that the maximum brush collapse attainable by appropriate choice of nanoparticle concentration is still significant (collapse by a factor of approximately 2 in the cylindrical brush system) but not as extensive as in the case of $\overline{v}$ = 1 nanoparticles.

The results presented in Figure 6 clearly indicate how the details of the brush collapse will depend on nanoparticle−monomer interaction strength and on nanoparticle size. It is also of interest to enquire about the effect of the brush grafting density on the brush morphology. In Figure 7 we show the SST approximation prediction for the brush height h versus c at three different grafting densities (namely σ = 0.0625, 0.08, and 0.1), all other parameter values being unchanged from the system considered in Figures 2−4. Clearly, the higher the grafting density, the less extensive the brush collapse. Conversely, lowering the grafting density should result in more extensive brush retraction from the cylinder center, at least within the brush regime of grafting densities. At sufficiently low grafting density, the grafted polymer system no longer forms a brush (strongly stretched chains), and SCF theory does not apply because for a very sparely grafted brush, lateral homogeneity of the brush is lost. Eventually, each chain forms a "mushroom" structure above its grafting point with no interchain interaction, and further decreasing the grafting density has little effect on the thickness of the polymer layer.

Downloaded by UNIV OF PITTSBURGH on September 3, 2015 | http://pubs.acs.org
Publication Date (Web): August 21, 2015 | doi: 10.1021/acs.jpcb.5b02623

DOI: 10.1021/acs.jpcb.5b02623
J. Phys. Chem. B 2015, 119, 11858−11866

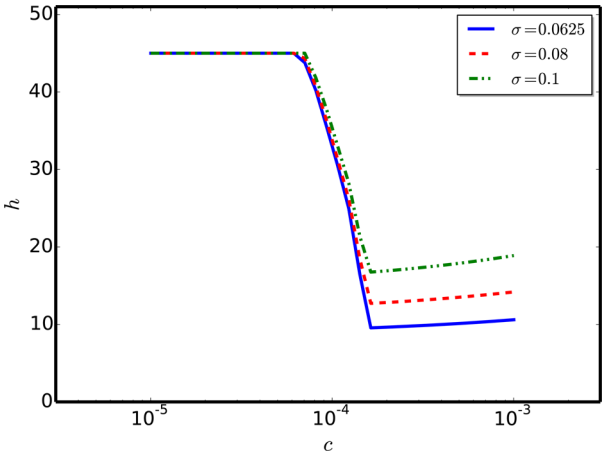

Figure 7. Effect of the grafting density on the brush collapse. Height h vs nanoparticle volume fraction c computed with SST for a cylindrically grafted brush with $R = 45$ and $\overline{\nu} = 1$, $\chi = -13.5$, $N = 100$, and grafting densities of $\sigma = 0.0625$, 0.08, and 0.1. Increasing the grafting density reduces the extent of the brush collapse.

Note that the location of the rapid collapse region as a function of nanoparticle concentration, c, is nearly independent of the brush grafting density, as is apparent in Figure 7. This is because in SST theory, $\mu(\psi)$ is independent of σ, so the range of nanoparticle concentrations in which there is an excisable van der Waals loop (cf. Figure 2) is also independent of σ. (As noted in connection with Figure 4 above, the rapid decrease of the brush height occurs within this range of concentrations.)

In Figure 8 we show for the cylindrically grafted $\overline{\nu} = 1$ brush simulation results for $\psi(r)$ and $\phi(r)$ for the case of $c = 10^{-4}$.

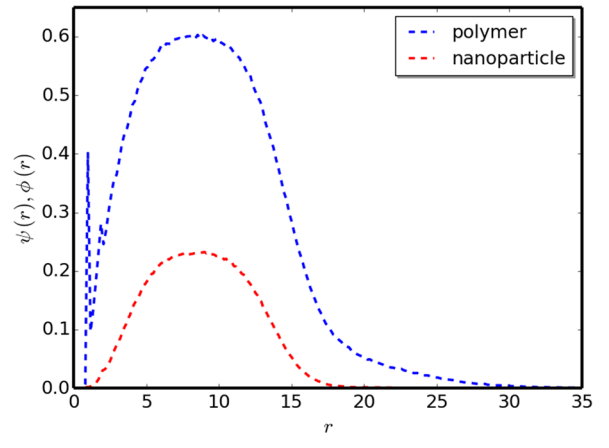

Figure 8. Monomer ("polymer") and nanoparticle ("nanoparticle") distributions in the channel obtained from Langevin simulations for a system with $\overline{\nu} = 1$, $N = 100$, $\varepsilon_b = 2$, $\sigma = 1/4^2 = 0.0625$, and $R = 45$ at the solution-phase nanoparticle concentration $c = 8.5 \times 10^{-5}$.

(Note that because $\overline{\nu} = 1$ here, ϕ is simply the number density of nanoparticles measured in units of b^{-3}.) The brush height attained in the simulation is close to the corresponding SST prediction (cf. Figure 3b). Again, the Langevin simulations tend to smooth out sharp features of the SST predictions (in this case, the sharp interface between densely packed and diffuse "micro"-phases revealed in the monomer density profile). Overall, however, the simulations validate the qualitative accuracy of the SST analysis for this system. The indicated nanoparticle distribution serves as a reminder that brush morphology changes are inherently concomitant with the absorption of nanoparticles into the brush. In the system under study here, it is apparent that the nanoparticles tend to localize strongly in the densely packed polymer core next to the grafting surface, with very few nanoparticles partitioning into the diffuse tail part of the brush, which is consistent with observations in previous work.[24] We also calculated the distribution of free chain ends (the location of the last monomer on the untethered end of the chain) for the system considered in Figure 8 and for several others (results not shown). In all cases, the distribution is nonzero over the entire extent of the brush, i.e., there are no "dead zones". The absence of the such zones is a prerequisite for the validity of the SST approximation.[27] Given the general success of the SST approximation in describing the behavior of the polymer brush−nanoparticle systems under study here, the absence of dead zones in the brush is not surprising.

4. DISCUSSION AND CONCLUSIONS

Polymer brushes can be assembled using a variety of polymeric materials, and the control of stimuli-responsive brushes is of paramount importance for nanotechnological applications. The nanovalve motif described in this paper is very general and relies on the basic properties of polymer−nanoparticle mixtures under confinement. Although we concentrated primarily on the case of $\overline{\nu} = 1$, the results shown in Figure 6 for $\overline{\nu} = 8$ (and also in ref 24) suggest that similar generic behavior is expected for larger nanoparticles, with the maximum magnitude and the sharpness of the brush collapse transition as a function the nanoparticle concentration occurring when $\overline{\nu} \approx 1$. Furthermore, although we have focused here on the *opening* of a polymer-occluded cylinder via nanoparticle infiltration, it is clear from Figure 6 and from previous work[23,24] that the valve can work in reverse. For example, given a polymer brush that has been maximally collapsed, further addition of nanoparticles will cause the brush to expand from that operating point. This suggests a way to precisely control *closure* of the nanovalve.

Of particular interest in the context of experimental verification of the nanovalve motif presented here are the unstructured polypeptide chains (nucleoporins) that occlude the pore of the nuclear pore complex (NPC) to large biomolecules. It has been suggested that conformational changes of these unfolded proteins induced by the binding of attractive transport proteins are responsible for NPC selectivity, although the detailed mechanism is still unclear.[13,46−49] Lim and co-workers have shown that the infiltration of planar brushes composed of unfolded nucleoporins by transport proteins that are attracted to them can cause collapse of the layer of variable magnitudes. Other recent experimental work[50] has identified specific hydrophobic anions that can serve as the nanoparticles infiltrating into the NPC, presumably driven by the attractive interactions between them and the hydrophobic and charged segments of the nucleoporin chains. The nanoparticles in this system are approximately the same size as the monomers of the polymer strands (a monomer being roughly one amino acid in the nucleoporin chain), in accord with the model considered here. The interpretation of these experiments indicates that the hydrophobic anion nanoparticles induce significant collapse of the layer of the unfolded proteins of the NPC.

Although the SST approximation has proven to be a versatile model of polymer brush statistical mechanics, it is far from exact. In a full simulation of the equilibrium state of an inwardly grafted cylindrical brush using, for example, a bead−spring

Downloaded by UNIV OF PITTSBURGH on September 3, 2015 | http://pubs.acs.org
Publication Date (Web): August 21, 2015 | doi: 10.1021/acs.jpcb.5b02623

DOI: 10.1021/acs.jpcb.5b02623
J. Phys. Chem. B 2015, 119, 11858−11866

Downloaded by UNIV OF PITTSBURGH on September 3, 2015 | http://pubs.acs.org
Publication Date (Web): August 21, 2015 | doi: 10.1021/acs.jpcb.5b02623

model of the polymer chains and additional beads (spheres) for the nanoparticles, we would expect that when the polymer chains extend into the center of the cylinder, they actually can cross the center point to some degree.[51,52] The extent to which they do so is best addressed by numerical simulations. In future work, we will thoroughly investigate the accuracy of the SST approximation for the problem under study here by conducting further coarse grained bead−spring Langevin dynamics simulations.[23,24,53] Such simulations will provide valuable information about the regime of the validity of SST theory for this class of system. They will also enable us to critically examine issues such as the effect of nanoparticle size on the brush collapse phenomenon and changes in equilibrium brush and nanoparticle morphologies due to cohesive properties of the brush (resulting from additional monomer−monomer interactions).[53,54] Ultimately, simulations of the same type will be carried out to directly study the flux of analyte molecules through the nanopore (by maintaining a nonzero analyte concentration in the reservoir abutting one of the caps and with an analyte sink in the reservoir abutting the other cap). In this way, we will be able to assess the real-time kinetics of the process as well as the possible complications of the expected flow mechanism. We cannot exclude from the equilibrium simulation results obtained here the possibility that there will be some analyte leakage through a "closed" brush valve, i.e., one which has no unoccluded volume as ascertained in the present work. Explicit nonequilibrium simulations will be required to determine whether this effect is significant.

Despite the desire for more extensive investigation of the morphological properties of this class of nanoparticle-infiltrated cylindrical brush systems, the calculations reported here provide novel insight into their behavior and establish an initial set of design principles that will be explored in future work and refined as necessary. In particular, small nanoparticles (with sizes close to the size of a monomeric unit of the polymer) with strong attraction to the polymer monomers generate sharp and significant collapse of the brush phase toward the cylindrical grafting surface. This creates significant free space (no polymer, only solvent) in the center of the cylinder (along the cylinder axis), allowing for the passage of larger analytes. The sharpness of the collapse with nanoparticle concentration in solution allows for precise control of the opening and closing of the valve. Conversely, larger nanoparticles and weaker nanoparticle−monomer binding energies diminish the degree of brush collapse and cause it to occur more gradually as nanoparticle concentration is varied.

Recent simulations of cylindrical brush motifs with cohesive brush ingredients indicate that such a brush is likely to favor extension into the cylinder center,[53,55] and that attractive nanoparticles may in that case form a plug of material in the center of the cylinder[53,56] rather than induce collapse of the brush toward the cylinder walls. To avoid the possibility that the brush filaments infiltrated with nanoparticles will form a plug of material in the center of the cylinder rather than collapsing toward the cylinder walls, our analysis suggests that utilizing noncohesive polymer molecules is advisible. Finally, the length of the polymer chains utilized is best chosen so that with the same grafting density in a planar brush system, the height of the pure brush (no nanoparticles) is approximately the radius of the cylinder used for the analogous cylindrical brush system. In such a system, the polymer chains in the pure brush cylindrical system will extend into the center of the cylinder but will not significantly interpenetrate through the cylinder center (interdigitate). In this way, we obtain the desired occlusion of the pore center without risking the unwanted trapping of polymer ends in the pore center.

AUTHOR INFORMATION

Corresponding Author

*Phone: (412) 624-8261. E-mail: coalson@pitt.edu.

Notes

The authors declare no competing financial interest.

ACKNOWLEDGMENTS

R.D.C. acknowledges support from the NSF grant CHE-1464551. A.Z. acknowledges support from the National Science and Engineering Research Council of Canada.

REFERENCES

(1) Currie, E. P. K.; Norde, W.; Cohen Stuart, M. A. Tethered polymer chains: Surface chemistry and their impact on colloidal and surface properties. *Adv. Colloid Interface Sci.* **2003**, *100−102*, 205−265.
(2) Milner, S. T. Polymer brushes. *Science* **1991**, *251*, 905−914.
(3) Galaev, I. Y.; Mattiasson, B. Smart polymers and what they could do in biotechnology and medicine. *Trends Biotechnol.* **1999**, *17*, 335−340.
(4) Minko, S. Responsive polymer brushes. *J. Macromol. Sci., Polym. Rev.* **2006**, *46*, 397−420.
(5) Balazs, A. C.; Emrick, T.; Russell, T. P. Nanoparticle polymer composites: Where two small worlds meet. *Science* **2006**, *314*, 1107−1110.
(6) Senaratne, W.; Andruzzi, L.; Ober, C. K. Self-assembled monolayers and polymer brushes in biotechnology: Current applications and future perspectives. *Biomacromolecules* **2005**, *6*, 2427−2448.
(7) Doi, M.; Edwards, S.F. *The Theory of Polymer Dynamics*. Oxford University Press: Oxford, England, 1988.
(8) Adiga, S. P.; Brenner, D. W. Flow Control through Polymer-Grafted Smart Nanofluidic Channels: Molecular Dynamics Simulations. *Nano Lett.* **2005**, *5*, 2509−2514.
(9) Milchev, A.; Dimitrov, D. I.; Binder, K. Polymer brushes with nanoinclusions under shear: A molecular dynamics investigation. *Biomicrofluidics* **2010**, *4*, 032202−8.
(10) Suo, T.; Whitmore, M. D. Controlling microtube permeability via grafted polymers and solvent quality. *J. Chem. Phys.* **2014**, *140*, 114902−7.
(11) Taunton, H. J.; Toprakcioglu, C.; Fetters, L. J.; Klein, J. Interactions between surfaces bearing end-adsorbed chains in a good solvent. *Macromolecules* **1990**, *23*, 571−580.
(12) Luzinov, I.; Minko, S.; Tsukruk, V. V. Responsive brush layers: From tailored gradients to reversibly assembled nanoparticles. *Soft Matter* **2008**, *4*, 714−725.
(13) Lim, R. Y. H.; Fahrenkrog, B.; Koser, J.; Schwarz-Herion, K.; Deng, J.; Aebi, U. Nanomechanical basis of selective gating by the nuclear pore complex. *Science* **2007**, *318*, 640−643.
(14) Iwata, H.; Hirata, I.; Ikada, Y. Atomic force microscopic analysis of a porous membrane with pH-sensitive molecular valves. *Macromolecules* **1998**, *31*, 3671−3678.
(15) Kowalczyk, S. W.; Kapinos, L.; Blosser, T. R.; Magalhaes, T.; van Nies, P.; Lim, R. Y. H.; Dekker, C. Single-molecule transport across an individual biomimetic nuclear pore complex. *Nat. Nanotechnol.* **2011**, *6*, 433−438.
(16) Lim, R. Y.; Deng, J. Interaction Forces and Reversible Collapse of a Polymer Brush-Gated Nanopore. *ACS Nano* **2009**, *3*, 2911−2918.
(17) Asatekin, A.; Gleason, K. K. Polymeric Nanopore Membranes for Hydrophobicity-Based Separations by Conformal Initiated Chemical Vapor Deposition. *Nano Lett.* **2011**, *11*, 677−686.
(18) Caspi, Y.; Zbaida, D.; Cohen, H.; Elbaum, M. Synthetic mimic of selective transport through the nuclear pore complex. *Nano Lett.* **2008**, *8*, 3728−3734.

(19) Javanovic-Talisman, T.; Tetenbaum-Novatt, J.; McKenney, A. S.; Zilman, A.; Peters, R.; Rout, M. P.; Chait, B. T. Artificial nanopores that mimic the selecticity of the nuclear pore complex. *Nature* **2009**, *457*, 1023−1027.
(20) Kohli, P.; Harrell, C. C.; Cao, Z.; Gasparac, R.; Tan, W.; Martin, C. R. DNA-functionalized nanotube membranes with single-base mismatch selectivity. *Science* **2004**, *305*, 984−986.
(21) Savariar, E. N.; Krishnamoorthy, K.; Thayumanavan, S. Molecular Discrimination Inside Polymer Nanotubules. *Nat. Nanotechnol.* **2008**, *3*, 112−117.
(22) Yameen, B.; Ali, M.; Neumann, R.; Ensinger, W.; Knoll, W.; Azzaroni, O. Ionic transport through single solid-state nanopores controlled with thermally nanoactuated macromolecular gates. *Small* **2009**, *5*, 1287−1291.
(23) Opferman, M. G.; Coalson, R. D.; Jasnow, D.; Zilman, A. Morphological control of grafted polymer films via attraction to small nanoparticle inclusions. *Phys. Rev. E* **2012**, *86*, 031806−7.
(24) Opferman, M. G.; Coalson, R. D.; Jasnow, D.; Zilman, A. The Morphology of Polymer Brushes Infiltrated by Attractive Nanoinclusions of Various Sizes. *Langmuir* **2013**, *29*, 8584−8591.
(25) Semenov, A. N. Contribution to the theory of microphase layering in block-copolymer melts. *J. Exp. Theor. Phys.* **1985**, *61*, 733−742.
(26) Zhulina, E. B.; Borisov, O. V.; Priamitsyn, V. A. Theory of steric stabilization of colloid dispersions by grafted polymers. *J. Colloid Interface Sci.* **1990**, *137*, 495−511.
(27) Milner, S. T.; Witten, T. A.; Cates, M. E. Theory of the grafted polymer brush. *Macromolecules* **1988**, *21*, 2610−2619.
(28) Kim, J. U.; Matsen, M. W. Compression of Polymer Brushes: Quantitative Comparison of Self-Consistent Field Theory with Experiment. *Macromolecules* **2009**, *42*, 3430−3432.
(29) Matsen, M. W. Corrections to the Strong-Stretching Theory of Polymer Brushes Due to the Entropy of the Free Ends. *J. Chem. Phys.* **2002**, *117*, 2351−2358.
(30) Dolan, A. K.; Edwards, S. F. The effect of excluded volume on polymer dispersant action. *Proc. R. Soc. London, Ser. A* **1975**, *343*, 427−442.
(31) Muthukumar, M.; Ho, J.-S. Self-consistent field theory of surfaces with terminally attached chains. *Macromolecules* **1989**, *22*, 965−973.
(32) Schmid, F. Self-Consistent-Field Theories for Complex Fluids. *J. Phys.: Condens. Matter* **1998**, *10*, 8105−8138.
(33) Milner, S. T. Strong-stretching and Scheutjens-Fleer descriptions of grated polymer brushes. *J. Chem. Soc., Faraday Trans.* **1990**, *86*, 1349−1353.
(34) Zhulina, E. B.; Borisov, O. V.; Pryamitsyn, V. A.; Birshtein, T. M. Coil-globule type transitions in polymers. I. Collapse of layers of grafted polymer chains. *Macromolecules* **1991**, *24*, 140−149.
(35) Ball, R. C.; Marko, J. F.; Milner, S. T.; Witten, T. A. Polymers grafted to a convex surface. *Macromolecules* **1991**, *24*, 693−703.
(36) Wijmans, C. M.; Zhulina, E. B. Polymer brushes at curved surfaces. *Macromolecules* **1993**, *26*, 7214−7224.
(37) Manghi, M.; Aubouy, M.; Gay, C.; Ligoure, C. Inwardly Curved Polymer Brushes: Concave Is Not Like Convex. *Eur. Phys. J. E: Soft Matter Biol. Phys.* **2001**, *5*, 519−530.
(38) Peleg, O.; Tagliazucchi, M.; Kroger, M.; Rabin, Y.; Szleifer, I. Morphology control of hairy nanopores. *ACS Nano* **2011**, *5*, 4737−4747.
(39) Flory, P. J. Thermodynamics of High Polymer Solutions. *J. Chem. Phys.* **1942**, *10*, 51−61.
(40) Grosberg, A. Y. and Khokhlov, A.R. *Statistical Physics of Macromolecules*; AIP Press: Columbus, OH; 1994.
(41) Wagner, M.; Brochard-Wyart, F.; Hervet, H.; de Gennes, P.-G. Collapse of polymer brushes induced by n-clusters. *Colloid Polym. Sci.* **1993**, *271*, 621−628.
(42) Binder, K. *Monte Carlo and Molecular Dyamics Simulations of Polymers*; Oxford University Press: Oxford, England, 1995.
(43) Tagliazucchi, M.; Szleifer, I. Stimuli-responsive polymers grafted to nanopores and other nano-curved surfaces: structure, chemical equilibrium and transport. *Soft Matter* **2012**, *8*, 7292−7305.
(44) Schneider, T.; Stoll, E. Molecular-dynamics study of a three-dimensional one-component model for distortive phase transitions. *Phys. Rev. B: Condens. Matter Mater. Phys.* **1978**, *17*, 1302−1322.
(45) Plimpton, S. Fast Parallel Algorithms for Short-Range Molecular Dynamics. *J. Comput. Phys.* **1995**, *117*, 1−19.
(46) Schoch, R. L.; Kapinos, L. E.; Lim, R. Y. Nuclear transport receptor binding avidity triggers a self-healing collapse transition in FG-nucleoporin molecular brushes. *Proc. Natl. Acad. Sci. U. S. A.* **2012**, *109*, 16911−16916.
(47) Lim, R. Y. H.; Huang, N. P.; Koser, J.; Deng, J.; Lau, K. H. A.; Schwarz-Herion, B.F. K.; Aebi, U. Flexible phenylalanine-glycine nucleoporins as entropic barriers to nucleocytoplasmic transport. *Proc. Natl. Acad. Sci. U. S. A.* **2006**, *103*, 9512−9517.
(48) Stewart, M. Molecular mechanism of the nuclear protein import cycle. *Nat. Rev. Mol. Cell Biol.* **2007**, *8*, 195−208.
(49) Wente, S. R.; Rout, M. P. The nuclear pore complex and nuclear transport. *Cold Spring Harbor Perspect. Biol.* **2010**, *2*, a000562−10.
(50) Kim, J.; Izadyar, A.; Shen, M.; Ishimatsu, R.; Amemiya, S. Ion Permeability of the Nuclear Pore Complex and Ion-Induced Macromolecular Permeation as Studied by Scanning Electrochemical and Fluorescence Microscopy. *Anal. Chem.* **2014**, *86*, 2090−2098.
(51) Dimitrov, D. I.; Milchev, A.; Binder, K. Polymer brushes in cylindrical pores: Simulation versus scaling theory. *J. Chem. Phys.* **2006**, *125*, 034905−15.
(52) Dimitrov, D. I.; Milchev, A.; Binder, K.; Heermann, D. W. Structure of Polymer Brushes in Cylindrical Tubes: A Molecular Dynamics Simulation. *Macromol. Theory Simul.* **2006**, *15*, 573−583.
(53) Ando, D.; Zandi, R.; Yong Woon, K.; colvin, M.; Rexach, M.; Gopinathan, A. Nuclear Pore Complex Protein Sequences Determine Overall Copolymer Brush Structure and Function. *Biophys. J.* **2014**, *106*, 1997−2007.
(54) Tagliazucchi, M.; Peleg, O.; Kroger, M.; Rabin, Y.; Szleifer, I. Effect of charge, hydrophobicity, and sequence of nucleoporins on the translocation of model particles through the nuclear pore complex. *Proc. Natl. Acad. Sci. U. S. A.* **2013**, *110* (9), 3363−8.
(55) Bestembayeva, A.; Kramer, A.; Labokha, A. A.; Osmanović, D.; Liashkovich, I.; Orlova, E. V.; Ford, I. J.; Charras, G.; Fassati, A.; Hoogenboom, B. W. Nanoscale stiffness topology reveals structure and mechanics of the tranport barrier in intact nuclear pore complexes. *Nat. Nanotechnol.* **2014**, *10*, 60−64.
(56) Osmanovic, D.; Ford, I. J.; Hoogenboom, B. W. Model Inspired by Nuclear Pore Complex Suggests Possible Roles for Nuclear Transport Receptors in Determining Its Structure. *Biophys. J.* **2013**, *105*, 2781−2789.

Downloaded by UNIV OF PITTSBURGH on September 3, 2015 | http://pubs.acs.org
Publication Date (Web): August 21, 2015 | doi: 10.1021/acs.jpcb.5b02623

DOI: 10.1021/acs.jpcb.5b02623
J. Phys. Chem. B 2015, 119, 11858−11866